Aalborg Universitet

A Decentralized Control Architecture applied to DC Nanogrid Clusters for Rural Electrification in Developing Regions

Nasir, Mashood; Jin, Zheming; Khan, Hassan; Zaffar, Nauman; Vasquez, Juan; Guerrero, Josep M.

A Decentralized Control Architecture applied to DC Nanogrid Clusters for Rural Electrification in Developing Regions

Mashood Nasir, Zheming Jin, Hassan A Khan, *Member, IEEE*, Nauman A. Zaffar, *Member, IEEE*, Juan. C. Vasquez, Senior *Member, IEEE* and Josep M.Guerrero, *Fellow, IEEE*

Abstract — **DC microgrids built through bottom-up approach are becoming popular for swarm electrification due to their scalability and resource sharing capabilities. However, they typically require sophisticated control techniques involving communication among the distributed resources for stable and coordinated operation. In this work, we present a communication-less strategy for the decentralized control of a PV/battery-based highly distributed DC microgrid. The architecture consists of clusters of nanogrids (households), where each nanogrid can work independently along with provisions of sharing resources with the community. An adaptive I-V droop method is used which relies on local measurements of SOC and DC bus voltage for the coordinated power sharing among the contributing nanogrids. PV generation capability of individual nanogrids is synchronized with the grid stability conditions through a local controller which may shift its modes of operation between maximum power point tracking mode and current control mode. The distributed architecture with the proposed decentralized control scheme enables a) scalability and modularity in the structure, b) higher distribution efficiency, and c) communication-less, yet coordinated resource sharing. The efficacy of the proposed control scheme is validated for various possible power sharing scenarios using simulations on MATLAB/Simulink and hardware in loop facilities at microgrid laboratory in Aalborg University.**

Index Terms — **DC Microgrid, DC Nanogrid, Distributed Generation, Distributed Storage, Droop Control, Rural-Electrification.**

I. INTRODUCTION

According to International Energy Agency (IEA), around 1.2 billion people (16% of the global population) do not have access to electricity. More than 95% of those living without electricity are the residents of sub-Saharan African and developing Asian countries, while around 80% of them reside in rural areas [1]. Electrification of these remote areas via national grid is unviable due to large up-front cost requirements. Electrification of these villages via islanded microgrids has seen an unprecedented growth in the recent years due to various factors mainly including a) lower up-front cost in comparison to national grid interconnection, b) successful business models for energy micro-financing, and c) advancements in power electronics, PV and battery technologies [2-4]. PV/battery-based DC microgrids have gain more popularity due to a) natural availability of solar energy in most of under-developed areas (most regions in Southeast Asia and Africa receive abundant sunlight i.e. above 5.5 kWhr/m^2/day), b) higher efficiency of DC distribution in comparison to AC distribution c) wide market availability and large penetration of highly efficient DC loads, d) gradually decreasing prices of PV panels and batteries, and e) omission of redundant AC/DC inter-conversion stages from generation to utilization [2, 5-8].

Prominent practical implementations for rural electrification through PV/battery-based islanded DC microgrids include micro-solar plants in Chhattisgarh, Sunderbans and Lakshadweep in India [9, 10]. Another very successful commercial scale project is Mera Gao Power (MGP) in India, where each subscriber may consume up to 5W of DC electricity (enough to power an LED light and a mobile-phone charging point) for 8-hrs per day. It is reported that MGP has over 10,000 subscribing households spread across 400 villages [11, 12]. The above-mentioned deployments utilize centralized architecture with top-down approach, where PV generation and battery storage is kept at a centralized location. This energy is delivered to subscribing households via distribution conductors and therefore, distribution losses are associated with the delivery of energy. The main advantage of central architecture is that power delivery can be controlled from a single point; therefore, this it offers simplicity in terms of operation, control and maintenance. However, this architecture is not readily scalable in terms of future expansions due to its non-modular nature. Further, distribution efficiency is a major limitation for centralized architectures, as distribution losses become significant at low distribution voltages, thin conductor sizes and higher power levels [13]. Moreover, such architectures require relatively higher initial capital investment due to top-down sizing requirements [14].

Various distributed architectures for PV/battery-based islanded DC microgrids have been proposed in literature. Distributed architectures with bottom-up approach enable

organic growth of microgrid, thereby, empowering local communities for sustainable development [14]. Wardah *et al.* [15] presented a partially distributed architecture, in which peer to peer electricity sharing was enabled by GSM based through power management units (PMU's). Similarly, Madduri *et al.* [16, 17] proposed a PV/battery-based central generation and distributed storage architecture, with the provision of local batteries in individual households. The advantages of distributed architectures are mainly reduction in distribution losses and modularity in structure. However, coordinated power sharing among the distributed resources becomes extremely challenging. Several strategies for hierarchical and supervisory control of DC microgrids have been proposed in [18-21]. However, these require an extra layer of sensing and communication, which enhances the cost and complexity of the system.

Thus, for PV/battery-based rural electrification, a distributed architecture having minimum distribution losses, modularly scalable structure and communication-less control is highly desirable. Mashood *et al.* [22] presented a PV-based distributed generation and distributed storage architecture (DGDSA) of DC microgrid for rural electrification. However, the hysteretic based voltage droop algorithm presented in [22] depends upon the perturbations in duty cycle. A very small perturbation in duty makes the dynamics of system very slow to achieve the desired power sharing, while a higher perturbation in duty cycle may lead to instability. In such a scheme, resource sharing capability among the distributed resources is uncoordinated i.e. all nanogrids share or demand uniform amount of power regardless of their current states generation and storage.

Xiaonan *et al.* [23] developed an adaptive dual loop droop control (inner current loop and outer voltage loop) on the basis of state of charge (*SOC*) balancing. This adaptive droop considers power sharing proportional to the battery *SOC* index during power supply mode (battery discharge mode). However, it does not consider power sharing in proportional to the *SOC* index during charging mode of the battery. Therefore, all batteries get charged with the same power independent of their state of charge or resource availability for battery charging. If such a scheme is applied on DGDSA of DC microgrid presented in [22] having local loads, there will be redundant distribution losses for un-wanted SOC balancing. Ideally, in such architectures, it is desirable that if *SOC* is above a certain threshold, it must be maintained to that level rather than undesired balancing. Moreover, *Zheming et al.* [24] showed that the V-I dual loop droop control exhibit slower dynamics in comparison to I-V droop, therefore, it cannot achieve fast power sharing among the distributed resources.

Therefore, in order to rectify these limitations of decentralized control schemes for distributed DC microgrids, we present an adaptive I-V droop method for the decentralized control of a PV-based DGDSA of DC microgrid suitable for rural electrification. The resource sharing among the contributing nanogrids is kept in proportion to the availability of resources for both operation modes i.e. during supply and demand of the power to or from the nanogrid (charging and discharging of the battery). This power sharing proportional to resource availability is achieved by using an adaptive I-V droop algorithm, which may adjust its droop based upon the local measurement of DC bus voltage and *SOC* of the battery. Moreover, the proposed control scheme ensures fast dynamics and is capable to deal with the extreme operating conditions by synchronizing PV generation capability of individual nanogrids with the local load requirements and grid stability conditions through a local controller, which may shift its modes of operation between MPPT mode and current control mode. Since, the proposed control scheme relies on the local measurements of load current, PV generation, battery *SOC* and DC bus voltage; therefore, does not require communication for the coordinated power sharing among the contributing nanogrids. Thus, with the proposed adaptive control scheme, PV based DGDSA combines the advantages of both of the existing architectures i.e. scalability, modularity, lower distribution losses, along with robust, coordinated and communication-less decentralized control. Thus, such a decentralized system can be considered as an ideal candidate for future deployments of rural electrification projects in developing regions.

The rest of this paper is organized as follows. In section II, the architecture of the proposed microgrid as an interconnection of multiple nanogrids is presented. In section III, power electronic interface and control schemes is presented. Section IV presents the objectives for various possible scenarios of coordinated control. Simulation and hardware results are presented in section V. Based upon the results and discussions, a conclusion is drawn in section VI.

II. DISTRIBUTED GENERATION AND DISTRIBUTED STORAGE ARCHITECTURE OF DC MICROGRID

The combination of PV generation, battery storage, local DC loads and DC-DC converters in an individual household formulates a nanogrid. Local generation and local storage allows the nanogrid to work independently even if the grid is unavailable and has many practical advantages compared to central generation based systems. A cluster of *N* multiple nanogrids is interconnected via a DC-link to formulate the distributed generation distribute storage architecture (DGDSA) of a DC microgrid as shown in Fig. 1. An individual nanogrid is therefore considered a basic building block, whose modular replication and subsequent DC-link integration yields scalability in the architecture. Each nanogrid operates independently when it is self-sufficient in its resources and resource sharing among multiple nanogrids is enabled only when an individual nanogrid has either access or deficiency of resources. Therefore, energy losses with the distribution of energy in DGDSA are limited in comparison to other partially distributed or centralized architectures, where generated energy has to be distributed all the way from centralized generation point to individual households [13, 22]. Further, DGDSA has the capability to aggregate power from multiple nanogrids for driving community loads. The supply of power for large communal loads is otherwise expensive and unsustainable in limited rural electrification projects [13, 22].
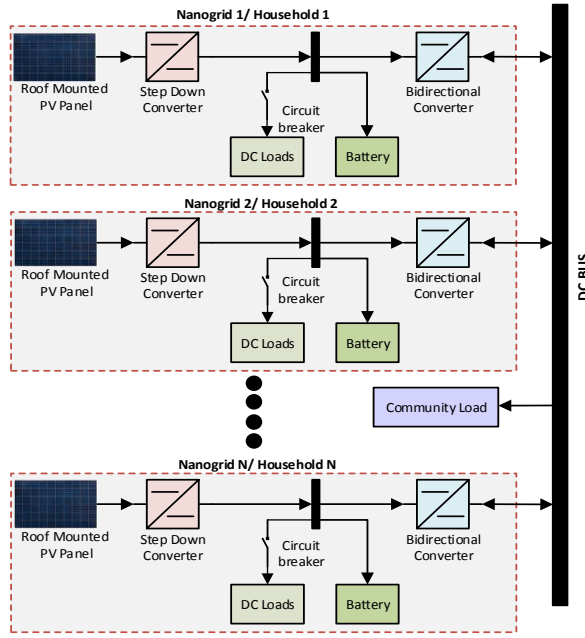
Fig. 1.   A cluster of multiple nanogrids interconnected via DC bus formulating the DGDSA of PV/battery-based DC microgrid.

III.   PROPOSED DECENTRALIZED CONTROL SCHEME FOR COMMUNICATION-LESS AND COORDINATED RESOURCE SHARING AMONG THE CLUSTER OF MULTIPLE NANOGRIDS

In the proposed decentralized scheme, each individual nanogrid is responsible for coordinated power sharing among the cluster without any physical communication. Power electronic interface for the formulation of an individual nanogrid is shown in Fig. 2a, which shows local PV generation, battery storage, household load and two DC-DC converters for power processing in an individual nanogrid. Index i is representing an arbitrary nanogrid in a cluster of N nanogrids. Battery acts as buffer between converter 1 of ith nanogrid ($Conv1_i$) and converter 2 of ith nanogrid ($Conv2_i$), and is responsible to keep the voltage fixed at the local bus to which household load is connected. Therefore, battery acts as a point of common coupling at which the terminals of load and both converters are connected. $Conv1_i$ is an isolated bidirectional converter and is responsible for controlled power sharing among nanogrids through interconnected DC bus. Distribution voltage in such low voltage direct current (LVDC) microgrids is dictated by DC bus voltage and is a key factor for achieving optimal distribution efficiency. Distribution at higher voltage is generally more efficient from the prospective of line losses and voltage drops at rear end [22]. Therefore, DC bus voltage is kept higher in comparison to battery voltage or household load voltage. This is achieved through converter ($Conv1_i$) which interfaces the battery with the DC bus. Moreover, to enable two-way power flow between battery of individual nanogrid and DC bus, this converter is made bi-directional in nature as shown in Fig.1 and Fig. 2. The advantage of making it as an isolated converter is twofold, i.e. a) it provides isolation between grid and battery and b) higher ratio of DC/DC voltage conversion can be achieved for implementing higher levels of LVDC,

i.e. 120V, 230V or 380V [22]. Converter 2 ($Conv2_i$) on the other hand is a step down converter and is responsible for optimal power extraction from PV panels.

The communication-less coordination among the distributed resources is achieved through the simultaneous control of each individual nanogrid via control scheme shown in Fig. 2b. The control scheme shown in Fig. 2b utilizes and adaptive algorithm (shown in Fig. 2c), for switching of $conv1_i$ based upon the local measurements of bus voltage V_B and battery state of charge SOC_i. This control scheme is also responsible for switching of $Conv2_i$ between MPPT and current control mode based upon the local measurements of household load, PV generation and battery SOC_i. Various possible modes of operation for $Conv1_i$ and $Conv2_i$ for each individual nanogrid as shown in Fig. 2c are discussed in the following subsections.

A.   Multi-mode Adaptive Control Scheme for Bidirectional Converter (Conv1i) Integrated with DC bus

For each nanogrid i, control mode for its bus interfaced converter $Conv1_i$ is determined by an adaptive controller on the basis of bus voltage V_B and state of charge of its battery SOC_i. The SOC_i of the battery is approximated by a simple Columb counting method, as governed by (1) and is based upon the ideal energy balance at i^{th} local bus given by (2):

$$SOC_i(t) = SOC_i(0) + \frac{1}{C_i}\int_0^T V_i^b\left(I_i^{in} - I_i^{load} - I_i^L\right)dt \quad (1)$$

$$P_i^{PV}(t)\Delta t = P_i^{load}(t)\Delta t + P_i^L(t)\Delta t + \int_0^T V_i^b\left(I_i^{in} - I_i^{load} - I_i^L\right)dt$$

$$(2)$$

Where, $SOC_i(0)$ is the initial state of charge for the battery at i^{th} nanogrid, C_i is its rated energy capacity (Wh), I_i^{in} is the current provided by PV panels after buck converter ($Conv2_i$), I_l^{load} is the current demanded by household DC loads, I_i^L is the current supplied by the nanogrid to the DC bus, $P_i^{PV}(t)$ is the power generated by PV panel at time t whose rated capacity is P^{PV} (W_p), $P_i^{load}(t)$ is the power demanded by household at time t whose rated load capacity is P^{load} (W) and $V_i^b(t)$ is the time varying voltage of the battery whose rated voltage is V_b. By convention I_i^L and P_i^L values are positive, when current and power is being supplied by the nanogrid to the DC bus and negative when current and power is being demanded by the nanogrid for household load or battery charging. In order to ensure the coordinated operation along with enhanced battery life time in each individual nanogrid, upper and lower threshold on the battery state of charge (SOC_i) are defined as SOC_{max} and SOC_{min}. SOC_i of the battery is considered as the resource availability index in the ith nanogrid, where, a value of SOC_i below SOC_{min} indicates that nanogrid is deficient in resources, a value of SOC_i above or equal to SOC_{max} indicates that nanogrid is saturated in resources and a value of SOC_i in between SOC_{max} and SOC_{min} indicates that nanogrid is self-sufficient. Similarly, in order to ensure the stability of the microgrid, a hysteresis is kept in the bus voltage V_B such that it is allowed to vary in between

± 5 % of the rated bus voltage V_{ref}, and associated higher and lower limits of voltage are denoted as V_H and V_L respectively. The local measurement of V_B at individual nanogrid serves as an indication for resource availability in the overall microgrid structure, where, a value lower than V_L indicates that cluster is deficient in resources, a value higher than or equal to V_H indicates that cluster is already saturated and a value in between V_L and V_H indicates that cluster has the capability of supplying as well as demanding power. Based upon the local measurements of SOC and V_B, an adaptive algorithm is used for the calculation of I_i^{ref} given by (4) - (11) and shown in Fig. 2c. An inner loop current control is then used to control the current of $Conv1_i$ (I_i^L) through PI controller that generates the duty cycle D_i given by (3), where, k_p and k_i are the proportional and integral constants for PI controller respectively. Based upon the local measurements of SOC_i and V_B, $Conv1_i$ of ith nanogrid can switch in the following modes as highlighted in Fig. 2c.

$$D_i = k_p \left(I_i^{ref} - I_i^L \right) + k_i \int_0^t \left(I_i^{ref} - I_i^L \right) dt \qquad (3)$$

1) Mode 1: Nanogrid is Deficient in Resources, while Cluster has Sufficient Resource Availability

A value of SOC_i below SOC_{min} indicates that i^{th} nanogrid is deficient in resources and any further discharge below this point will deteriorate the battery life. So, individual household loads are shut down with a relay and it starts absorbing power to achieve the minimum sustainability level i.e. SOC_{min}. A value of V_B higher than reference voltage V_{ref} indicates that neighboring nanogrids have enough capability to serve for the demand of resource deficient nanogrids. In this situation, resource deficient nanogrids will demand power in accordance to their resource deficiency. The current reference I_i^{ref} varies with SOC_i in a linear fashion from $SOC_i=0$ to SOC_{min} as shown in Fig. 2c (Mode 1) and is given by (4). From (4) and Fig. 2c (Mode 1), it is evident that the battery of resource deficient nanogrid will get charged with rated current I_{rated} at $SOC_i =0$, and power delivery will become eventually zero with $I_i^{ref}=0$ as SOC_i approaches to SOC_{min}. Where, I_{rated} is the rated charging current for the battery, specified by manufacturer datasheet.

$$I_i^{ref} = I_{rated} \left(\frac{SOC_i}{SOC_{min}} - 1 \right); \forall i \in [1, N] \text{ if } V_B > V_L \qquad (4)$$

2) Mode 2: Nanogrid and Cluster, Both are Deficient in Resources

A value of SOC_i below SOC_{min} and V_B less than or equal to V_L indicates that i^{th} nanogrid is deficient in resources, while neighboring nanogrids in the cluster do not have the capability to serve for the demand of resource deficient naogrids, Therefore, to avoid any further drop in DC bus voltage, each $Conv1_i$ will adjust its reference current to stabilize DC bus voltage at lower allowable limit i.e. V_L. This coordination is achieved through the virtual droop resistance R_d of the converter and is given by (5) (also shown in Fig. 2c

(Mode 2)). From (5) and Fig. 2c (Mode 2), it is evident that once DC bus voltage stabilizes at lower allowable limit i.e. V_L, net exchange of power between multiple nanogrids will become zero with $I_i^{ref} = 0$.

$$I_i^{ref} = \frac{1}{R_d} \left(V_L - V_B \right); \forall i \in [1, N] \text{ if } V_B \leq V_L \qquad (5)$$

3) Mode 3: Nanogrid is Saturated, while Cluster is Unsaturated in Resources

A value of SOC_i higher than SOC_{max} , indicates that i^{th} nanogrid has very high resource availability and it needs to supply power to the neighboring nanogrids. If the bus voltage V_B is lower than V_H, it indicates that cluster is unsaturated in resources and neighboring nanogrids can absorb power; therefore, each $conv1_i$ will supply power to the cluster. The current reference I_i^{ref} varies with SOC_i in a linear fashion from SOC_{max} to $SOC= 100\%$ as shown in Fig. 2c (Mode 3) and is given by (6). From (6) and Fig. 2c (Mode 3), it is evident that the battery of saturated nanogrid will be discharged with rated current I_{rated} at $SOC_i =100$, and power delivery will become eventually zero with $I_i^{ref}=0$ as SOC_i approaches to SOC_{max}.

$$I_i^{ref} = I_{rated} \left(\frac{SOC_i - SOC_{max}}{100 - SOC_{max}} \right); \forall i \in [1, N] \text{ if } V_B < V_H \qquad (6)$$

4) Mode 4: Nanogrid and Cluster, both are Saturated in Resources

A value of SOC_i above SOC_{max} and V_B higher than or equal to V_H indicates that i^{th} nanogrid is saturated in resources, while neighboring nanogrids in the cluster are already saturated. Therefore, in this condition, to avoid increase in DC bus voltage, each $Conv1_i$ will adjust its reference current to stabilize DC bus voltage at higher allowable limit i.e. V_H. This coordination is achieved through the virtual droop resistance R_d of the converter and is given by (7) (also shown in Fig. 2c (Mode 4)). From (7) and Fig. 2c (Mode 2), it is evident that once DC bus voltage stabilizes at higher allowable limit i.e. V_H, and net exchange of power between multiple nanogrids will become zero with $I_i^{ref} = 0$.

$$I_i^{ref} = \frac{1}{R_d} \left(V_H - V_B \right); \forall i \in [1, N] \text{ if } V_B \geq V_H \qquad (7)$$

5) Mode 5: Nanogrid is self-sufficient, while Cluster can Supply or Demand Resources,

For i^{th} nanogrid, value of SOC_i in between SOC_{max} and SOC_{min} indicates that it is self-sufficient in resources. In this condition, it can either supply power to the cluster, it can demand power from the cluster or it can work independently without any exchange of power among the neighboring nanogrids in the cluster. If all the nanogrids in the cluster are self-sufficient, there is no exchange of power among neighboring naogrids and voltage is stabilized at V_{ref} through adaptive I-V droop control.
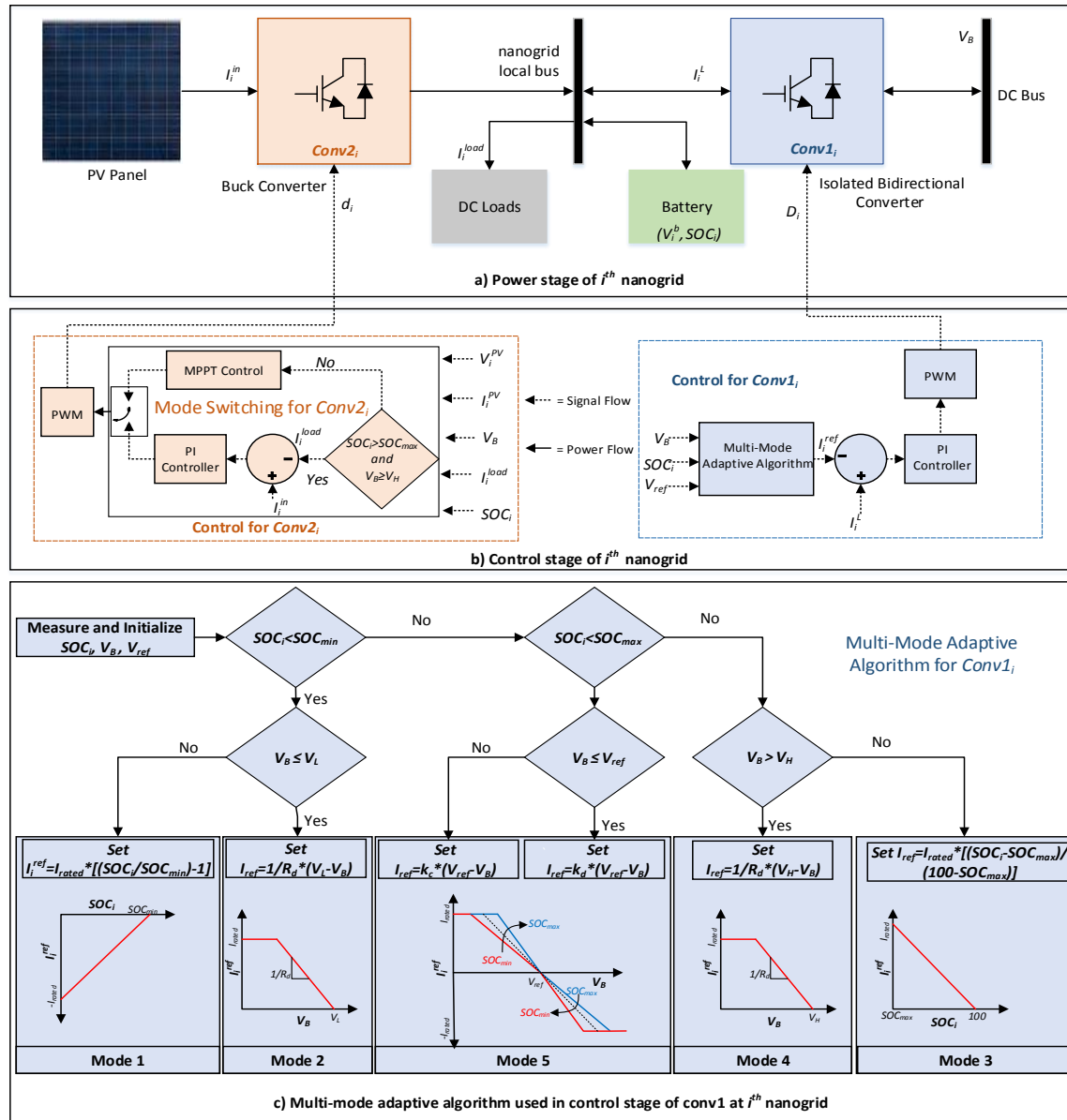
Fig. 2. Power electronic interface and control schemes for an individual nanogrid to achieve desired decentralized coordinated power sharing

A value of V_B higher than V_{ref} indicates that number of power supplying nanogrids in the cluster is more than number of power demanding nanogrids, therefore, i^{th} nanogrid needs to absorb power to keep the microgrid stable. The coordinated power absorption in this condition is achieved through an adaptive I-V droop control given by (8) and shown in Fig.2c (Mode 5). Rather than having a fixed value of droop resistance, a charging droop coefficient K_c has been defined as a function of droop resistance R_d and SOC_i given by (9). For $SOC_{min} < SOC_i < SOC_{max}$,

$$I_i^{ref} = K_c \left(V_{ref} - V_B \right); \ \forall i \in [1, N] \ \text{if} \ V_B > V_{ref} \qquad (8)$$

$$K_c \left(R_d, SOC_i \right) = \frac{1}{R_d} \left(2 - \frac{SOC_i - SOC_{min}}{SOC_{max} - SOC_{min}} \right) \qquad (9)$$

A higher value of droop coefficient at SOC_{min} and a lower value of droop coefficient at SOC_{max} results in a coordinated power absorption such that nanogrid with lowest state of charge absorbs highest amount of power from the cluster and vice versa. The proposed scheme employs an adaptive I-V droop method for the control of microgrid. Although, current based droop control (I-V droop) exhibits better transient performance in comparison to other droop methods (e.g. V-I droop), however, it may be subjected to instability, if droop coefficient is kept too high [25]. The upper and lower boundary conditions for the stability of I-V droop controlled microgrids and a design criterion for global droop coefficient ensuring system stability for wide range operation has been discussed in [25]. It has been shown that stability margins of the system increase with the increase in DC-link capacitance, decrease in feeder inductance and decrease in load power [25]. Since, the proposed distribution architecture is designed for the limited electrification needs of rural occupants with

smaller distribution radius (standard size of a village is less than a km), therefore, due to high link capacitance, low feeder inductance and low power loads, stability margins are relatively higher. The droop coefficient in the proposed adaptive scheme has been varied linearly from $2/R_d$ to $1/R_d$ between SOC_{min} to SOC_{max}, and lies within the stable boundaries as discussed in [25]. Other linear and non- non-linear variations of droop function can be considered in the proposed approach without losing stability, subject to the conditions for droop coefficient design in [25].

A value of V_B lower than V_{ref} indicates that number of power demanding nanogrids in the cluster is more than number of power supplying nanogrids, or there is a communal load demand, therefore, i^{th} nanogrid needs to supply power to keep the microgrid stable. The coordinated power sharing among the supplying nanogrids is ensured through modified I-V droop control given by (10) and shown in Fig. 2c (Mode 5). For this range, a discharging droop coefficient K_d has been defined based upon the same criteria discussed above.

$$I_i^{ref} = K_d\left(V_{ref} - V_B\right); \ \forall i \in [1, N] \ \text{if} \ V_B \leq V_{ref} \qquad (10)$$

$$K_d\left(R_d, SOC_i\right) = \frac{1}{R_d}\left(1 + \frac{SOC_i - SOC_{min}}{SOC_{max} - SOC_{min}}\right) \qquad (11)$$

The variations in droop coefficient with SOC_i ensure that nanogrid with highest resource availability (higher value of SOC) will supply more power in comparison to the nanogrid having relatively lower value of SOC.

B. Scheme for switching between MPPT and Current Control Modes for the Converter Integrated with PV Panel (Conv2i)

The buck converter of each nanogrid ($Conv2_i$) at the output of PV panel is responsible for optimal battery charging. Maximum power point tracking (MPPT) control is widely used in PV based systems for the extraction of maximum power out of incident solar energy. Various schemes for MPPT under uniform and non-uniform irradiance have been discussed in the literature [26, 27]. In this article, the perturb and observe algorithm is employed due to its simplicity and low computational complexity [26]. The algorithm processes PV panel voltage V_i^{PV} and current I_i^{PV} to generate duty cycle *di* for maximum power extraction from PV panel at a given solar irradiance. In most of its operation range $Conv2_i$ will operate in MPPT mode however, based upon the measurements of SOC_i and V_B, $Conv2_i$ may shift its operation from MPPT mode to inner loop current control mode to culminate its power generation from MPPT to household load current requirements I_i^{load} only. Thus, for $SOC_i > SOC_{max}$ and $V_B \geq V_H$, $Conv2_i$ will operate in inner loop current control mode through a PI controller that will generate duty cycle d_i given by (12), where, $k_P{}'$ and $k_i{}'$ are proportional and integral constants of PI controllers employed for the control of $conv2_i$.

$$d_i = k_p{}'\left(I_i^{load} - I_i^{in}\right) + k_i{}'\int_0^t \left(I_i^{load} - I_i^{in}\right)dt \qquad (12)$$

IV. Objectives for Stable and Coordinated Operation

For stable operation of the microgrid, DC bus voltage V_B must be maintained to rated value V_{ref} with some allowed fluctuation (±5%) in bus voltage for all possible operating conditions. The other control objective is to minimize the overall distribution losses, while maintaining a coordinated resource sharing among the nanogrids. The proposed decentralized scheme will ensure the stable and coordinated operation in the following possible scenarios:

a) Each nanogrid is self-sufficient in its resources i.e. PV generation/battery cushion is in accordance with household load requirements, and any exchange of power among nanogrids is not desirable to minimize the distribution losses. This will be achieved through the operation of each $conv1_i$ in Mode 5 and each $conv2_i$ in MPPT mode.

b) Although each nanogrid is self-sufficient in its resources, but there is a communal load demand on the microgrid. In this case it is desireable that each individual nanogrid contribute power for communal load operation in proportion to its resources availability. This will be achieved through the operation of each $conv1_i$ in Mode 5 and each $conv2_i$ in MPPT mode.

c) Out of total *N* nanogrids, *K* nanogrids are self-sufficient while *N-K* nanogrids are deficient in resources. In this case, it is desireable that *K* self-sufficient nanogrids share their resources with the remaining *N-K* resource deficient nanogrids in a coordinated fashion such that the nanogrid with highest resource availability should supply more power in comparison to the rest of self-sufficient nanogrids and the nanogrid with the highest resource deficiency should receive more power in comparison to the rest of deficient nanogrids. In this situation, $Conv1_i$ of *K* self-sufficient nanogrids will be operating in Mode 5, while, remaining *N-K nanogrids* will be operating in Mode 1. $Conv2_i$ of all *N* nanogrids will be operating in MPPT Mode.

d) Out of total *N* nanogrids, *K* nanogrids are self-sufficient while *N-K* nanogrids are deficient in resources and there is a communal load demand. In this case, it is desireable that *K* self-sufficient nanogrids share their resources with the remaining *N-K* resource deficient nanogrids in a coordinated fashion and communal load demand is also met such that the nanogrid having highest resource availability supply more power and vice versa. In this situation, $Conv1_i$ of *K* self-sufficient nanogrids will be operating in Mode 5, while, remaining *N-K nanogrids* will be operating in Mode 1. $Conv2_i$ of all *N* nanogrids will be operating in MPPT Mode.

e) Out of total *N* nanogrids, *K* nanogrids are self-sufficient while *N-K* nanogrids are saturated in resources. In this case, it is desireable that *K* self-sufficient nanogrids absorb power from the remaining *N-K* resource saturated nanogrids in a coordinated fashion such that the nanogrid with lowest resource availability absorb more power and vice versa. In this situation, $Conv1_i$ of *K* self-sufficient nanogrids will be operating in Mode 5, while, remaing *N-K nanogrids* will be operating in Mode 3. $Conv2_i$ of all *N* nanogrids will be operating in MPPT Mode.

TABLE I
PARAMETERS OF SIMULATED CASE STUDY

Description of the Parameter	Symbol	Value	Description of the Parameter	Symbol	Value
No. of Nanogrids/ households	N	4	Maximum threshold of battery SOC	SOC_{max}	80%
DC bus capacitance	C_B	10mF	Minimum threshold of battery SOC	SOC_{min}	30%
Inductance of each $Conv1_i$	L_1	500μH	Reference voltage for DC bus	V_{ref}	48V
Switching frequency for $Conv1i$ and $Conv2i$	f_{sw}	10kHz	Initial Voltage of DC bus	V_{B0}	24V
Rated power of each PV panel	P^{PV}	500W$_p$	Lower limit on DC bus voltage	V_L	45.6V
Rated household load	P^{load}	200W	Higher limit on DC bus voltage	V_H	50.4V
Battery capacity for each nanogrid	C	2400Wh	Droop Coefficient for $Conv1_i$	R_d	0.218Ω
Rated Charging current for the battery	I_{rated}	10A	Proportional and integral parameters ($Conv1_i$)	k_p,k_i	0.33, 15
Rated voltage of each battery	V^b	24V	Proportional and integral parameters ($Conv2_i$)	k_p,k_i	0.5, 50

f) All the nanogrids are generating more power than their local requirements i.e. excess power is available after fulfilling household load requirements and battery capacity. Although this situation can be largely avoided by optimaly designing PV generation and battery storage resources [28]. Still, even a single occurance of this situation may instigate grid instability. In this case, it is desireable to culminate the PV generation and synchronise it with houshold load requirements. In this situation, $Conv1_i$ of all N nanogrid will be operating in Mode 4 and $Conv2_i$ of all N nanogrids will be operating in current control mode.

g) All nanogrids are deficient in resources and they start demanding power, which may result in grid voltage drop below specified tolerance and subsequent instability. In this situation it is desitreable that all household loads are shed and there is no power sharing with the common DC bus, until the batteries are recharged again when PV reources are available. In this situation, $Conv1_i$ of all N nanogrid will be operating in Mode 2 and $Conv2_i$ of all N nanogrids will be operating in MPPT mode.

V. RESULTS AND DISCUSSIONS

For the validation of proposed scheme various test cases are analyzed via simulations and hardware in loop (HIL).

A. Simulation Results for Decentralized Control

Simulations are carried out on MATLAB/Simulink using physical models of the converters and control schematic shown in Fig. 2a. Various parameters for simulation are shown in Table I. In order to have a better illustration of results, $P_i^{PV}(t)$ is assumed equal to $P_i^{load}(t)$ for test cases 1, 2 and 3.

1) All nanogrids are within specified thresholds of SOC

In order to validate the scenarios *a* and *b* of section IV, batteries of all nanogrids are assumed to be within specified thresholds, i.e. $SOC_{min} \leq SOC_i \leq SOC_{max}$; $\forall i=1,2, 3, 4$. This case is evaluated with and without communal load. Results for variations in bus voltage, current sharing among nanogrids and accelerated simulations (0.5 hr) for SOC_i are shown in Figs. 3a and 3b respectively. After starting transient, if there is no communal load, current sharing among the nanogrids is almost zero, i.e. each nanogrid is working independently, without supplying or demanding power from DC bus. So, their SOC's remain constant in this

region and distribution losses are zero, despite load requirements of each household is being fulfilled.

At $t= 0.025$ s, a communal load of 500 W is applied due to which voltage of the DC bus drops from 48 V to 47.3 V and each nanogrid starts contributing for communal load based upon its availability index i.e. SOC_i value. Therefore, all nanogrids are supplying power based upon the modified droop $K_d(R_d, SOCi)$ given by (11) and Fig. 2c (Mode 5). Consequently, the nanogrid with highest SOC, contributes more towards communal load and its SOC decreases at a rapid slope in comparison to other nanogrids ($\Delta SOC_1 = 1.92\%$ in comparison to $\Delta SOC_4 = 2.52\%$ at the end of simulation). Moreover, as discussed by Zheming *et. al* [24], I-V droop exhibit superior transient performance in comparison to other droop methods (e.g. V-I droop), therefore, transition from one mode to other is smooth. From Fig. 3a, it is evident that upon the application of communal load at $t=0.025$ s, the proposed control achieves the new steady state in less than 0.005 s with negligible ringing or overshoot in converter current and DC bus voltage.
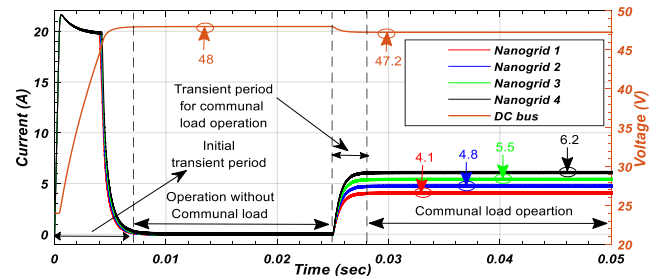

Fig. 3a. DC bus voltage V_B profile (righy Y-axis) and current sharing among nanogrids (I_1^L, I_2^L, I_3^L and I_4^L) (left Y -axis) in case 1 (simulation results)
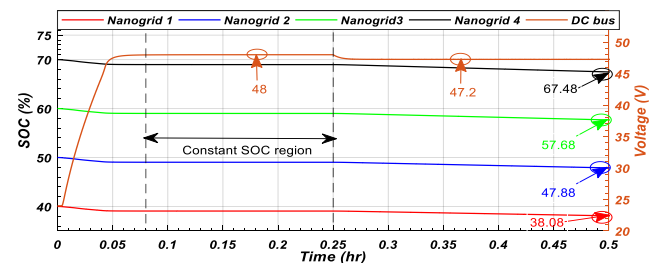

Fig. 3b. DC bus voltage V_B profile (righy Y-axis) and battery SOC for contributing nanogrids (SOC_1, SOC_2, SOC_3 and SOC_4) (left Y-axis) in case 1 (simulation results)

2) Two nanogrids are within specified thresholds of SOC, while remaining two are below threshold of SOC.

In order to validate the scenarios *c* and *d* of section IV, the batteries of two nanogrids are assumed to be within specified thresholds of *SOC,* while the batteries of remaining two nanogrids are assumed to be below threshold of *SOC,* i.e. $SOC_i < SOC_{min}$; $\forall i=1,2$; $SOC_{min} \leq SOC_j \leq SOC_{max}$; $\forall j=3,4$. This case is evaluated with and without communal load and results for variations in bus voltage, current sharing among contributing nanogrids and accelerated simulations (0.5 hr) for SOC_i are shown in Figs. 4a and 4b respectively.

Moreover, to visualize the accuracy of power sharing, two self-sufficient nanogrids are assumed to be having same value of initial *SOC* i.e.70%. It can be seen that after starting transient, if there is no communal load, deficient nanogrids are demanding power in accordance to (4), also shown in Fig. 2c (Mode 1). Self-sufficient nanogrids are supplying power to the deficient nanogrids in accordance to (11) and Fig. 2c (Mode 5).

Since, power sharing is based upon *SOC* value only, therefore, two nanogrids having same value of *SOC*, share exactly the same currents as evident by overlapping lines in Fig. 4a and 4b respectively. At *t*= 0.025 s, a communal load of 500 W is applied due to which voltage of the DC bus drops from 47.3 V to 46.5 V and self-sufficient nanogrids start contributing for communal load as well as power demand of deficient nanogrids. Since, deficient nanogrids are demanding power in proportion to their deficiency, thereby, nanogrid having lower value of initial *SOC* is being charged at higher current and vice versa. (ΔSOC_1 = 0.68% in comparison to ΔSOC_2 = 0.45% at the end of simulation).
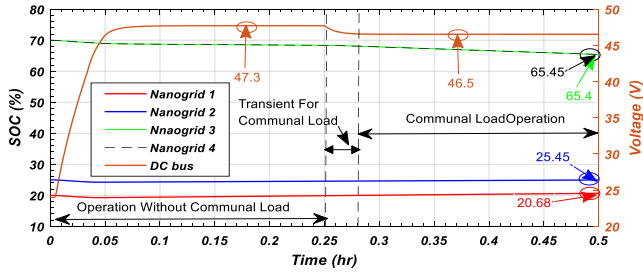
3) All nanogrids are within specified thresholds of SOC except one which is above maximum threshold of SOC

In order to validate the scenario *e* of section IV, the batteries of three nanogrids are assumed to be within specified thresholds of *SOC,* while battery of fourth nanogrid is above maximum threshold of *SOC*, i.e. $SOC_{min} \leq SOC_j \leq SOC_{max}$. ; $\forall i=1, 2, 3$; $SOC_4 > SOC_{max}$. Results for bus voltage profile, current sharing among contributing nanogrids and accelerated simulations (1 hr) for SOC_i is shown in Figs. 5a and 5b respectively.

Since the initial $SOC_4^{(0)}$ is above threshold i.e. 90%, therefore, in this scenario, nanogrid 4 is supplying power as dictated by (6), also shown in Fig. 2c (Mode 3) with I_1^L=4.98A, while other three are absorbing power (their batteries are being charged) based upon the modified droop $K_c(R_d, SOCi)$ given by (9) and Fig. 2c (Mode 5).

It can be observed from Figs. 5a and 5b that power sharing via modified droop ensures resource distribution based upon the availability index. Therefore, nanogrid with initial $SOC_3^{(0)}$ =75% (highest SOC and highest resource availability) is being charged with the lowest current I_3^L = -1.28A in comparison to nanogrid with $SOC_2^{(0)}$= 55% and nanogrid with $SOC_2^{(0)}$= 35% which are being charged at I_2^L=-1.73A and I_3^L =-2.18A respectively. Moreover, the changes in SOC_i from start till end of the simulation are also in accordance with the modified droop, such that the nanogrid with highest resource availability is being discharged at the highest rate, while nanogrid 3 with minimum resources availability is being charged at lowest rate with ΔSOC_1=0.96%, ΔSOC_1=0.49% and ΔSOC_1=0.2% respectively ($\Delta SOC_1 < \Delta SOC_2 < \Delta SOC_3$).

Fig. 4b. DC bus voltage V_B profile (righy Y-axis) and battery *SOC* for contributing nanogrids (SOC_1, SOC_2, SOC_3 and SOC_4) (left Y-axis) in case 2 (simulation results)
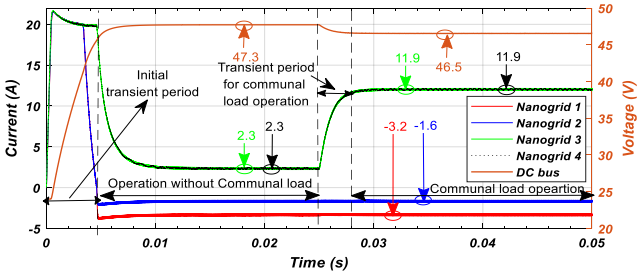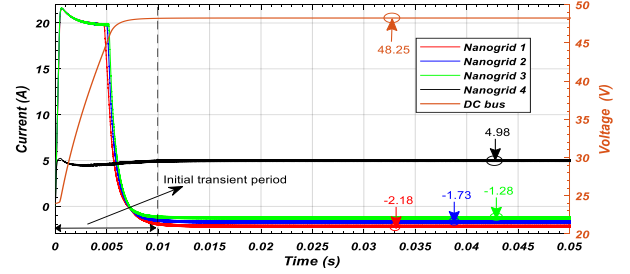

Fig. 5a. DC bus voltage V_B profile (righy Y-axis) and current sharing among nanogrids (I_1^L, I_2^L, I_3^L and I_4^L) (left Y-axis) in case 3 (simulation results)

Fig. 4a. DC bus voltage V_B profile (righy Y-axis) and current sharing among nanogrids (I_1^L, I_2^L, I_3^L and I_4^L) (left Y -axis) in case 2 (simulation results)
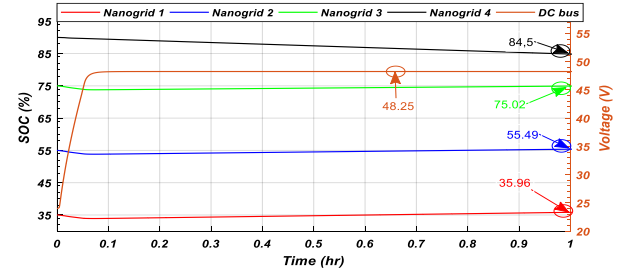

Fig. 5b. DC bus voltage VB profile (right Y-axis) and battery SOC for contributing nanogrids (SOC1, SOC2, SOC3 and SOC4) (left Y-axis) in case 3 (simulation results)

4) Multi-mode switching of an individual nanogrid

In order to realize the working of an individual nanogrid in all possible threshold ranges and to visualize the multi-mode switching based upon the *SOC* thresholds, nanogrids 2,3 and 4 are considered to be working within specified maximum and minimum thresholds of *SOC* with $SOC_2<SOC_3<SOC_4$, while, nanogrid 1 is considered below threshold in the start of simulation. It is assumed that PV power produced within the first three nanogrids is in accordance with their household loads; while incident irradiance and associated PV power produced within nanogrid 1 is higher than its household load requirements. Therefore, based upon the energy balance given in (1) and (2), SOC_1 will increase from values below SOC_{min} to values above SOC_{max}, Consequently, $Conv1_1$ will switch its operating modes accordingly.

Fig. 6 shows the variations in current sharing among contributing nanogrids (I_1^L, I_2^L, I_3^L and I_4^L) based upon the accelerated *SOC* variations of an individual nanogrid (SOC_1). Accelerated SOC variations at nanogrid 1 are achieved by considering reduced battery capacity ($C/5$) and high incident irradiance (1000W/m^2). It can be observed that when $SOC_1<SOC_{min}$, nanogrid 1 is demanding current with negative value of I_1^L as dictated by equation (4). Current demanded by naogrid 1, I_1^L decreases as *SOC* increases and becomes almost zero, when it reaches to minimum threshold point at $SOC_1 =30\%$ in accordance with Fig. 2c (Mode 1). It is worth noting that within this range of operation, the current supplying capability of the remaining three microgrids is governed by the modified discharging droop $K_d(R_d, SOC_i)$ given by equation (11) and its visual representation is also shown in Fig. 2c (Mode 5), such that nanogrid 4 having highest *SOC* is supplying maximum current, while nanogrid 2, having lowest *SOC* is supplying lower current. In mid operation range, i.e. within specified limits of thresholds, all nanogrids are sharing zero current, therefore, in this range distribution losses are comparatively negligible. Also, it is evident from Fig. 6 that the inter-mode transition is very fast and smooth with the proposed strategy. For $SOC_1>SOC_{max}$, nanogrid starts supplying current in accordance with (6) and Mode 3 of Fig. 2c, therefore, value of I_L^1 keeps on increasing with increase in SOC_1. In this mode of operation, the current sharing of remaining three microgrids is controlled by modified charging droop $K_c(R_d, SOC_i)$ given by equation (9) and its visual representation is also shown in Fig. 2c (Mode 5).
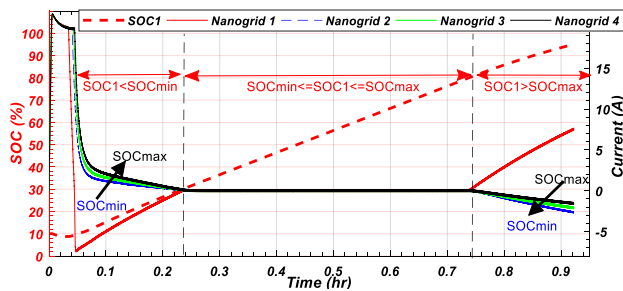
5) All nanogrids are above maximum threshold of SOC and surplus PV power is available

To validate the scenario *f* of section IV, it is considered that all the nanogrids are above maximum threshold and surplus PV power is available due to high incident irradiance (1000W/m^2) i.e. $SOC_i > SOC_{max}$; $\forall i=1, 2, 3, 4$. Each naogrid will tend to supply power to the DC bus based upon the equation (6), therefore, its voltage will rise until it reaches to V_H. At V_H, the proposed droop function given by (7), also shown in Fig. 2c (Mode 4) will reduce the current supply to zero and will try to keep the voltages fixed at V_H. Since, the batteries are already above maximum threshold, therefore, any local PV generation P_i^{PV}, higher than local household requirements P_i^{load} will overcharge the battery and cause DC bus voltage to rise above the maximum limit V_H, thus instigating instability in the system. At this point, the control schematic of $conv2_i$ changes its control from MPPT to inner loop current control mode as shown in Fig. 2c. Therefore, I-V droop control mode (constant droop coefficient R_d) of $Conv1_i$ stabilizes the DC bus voltage at V_H and $Conv2_i$ ensures stability by culminating generation capability of each nanogrid according to the load requirements at individual household level. Fig. 7a shows that when DC bus voltage is below maximum threshold V_H, each nanogrid contributes for current according to its SOC_i. Once the voltage reaches to V_H, current contribution from each nanogrid becomes zero, and further rise in voltage is restricted to V_H. Before attaining V_H, each $Conv2_i$ is operating in MPPT mode, thus extracting maximum power (500 W at incident irradiance of 1000 W/m^2). However, once DC bus voltage attains its maximum value V_H, the PV generation is limited according to household load requirements.
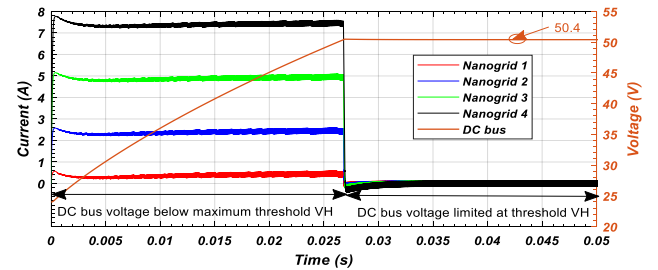

Fig. 7a. DC bus voltage V_B profile (righy Y-axis) and current sharing among nanogrids (I_1^L, I_2^L, I_3^L and I_4^L) (left Y-axis) in case 5 (simulation results)
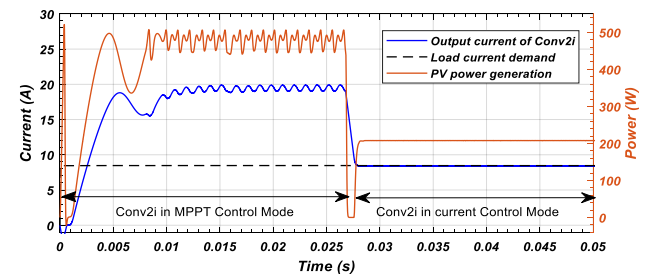

Fig. 7b. Power generated by PV panels in nanogrid 1 P_1^{PV} (righy Y-axis) and output current I_1^{in} of $conv2_1$(left Y-axis) in case 5 (simulation results)
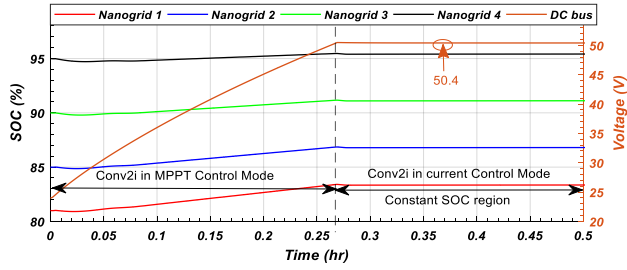

Fig. 6. Nanogrid 1 SOC_1 variation in the various thresholds ranges (left Y-axis) and associated current sharing among the contributing nanogrids in case 4 (right Y- axis) (simulation results)

Fig. 7c. DC bus voltage V_B profile (righy Y-axis) and battery SOC for contributing nanogrids (SOC_1, SOC_2, SOC_3 and SOC_4) (left Y-axis) in case 5 (simulation results)

This is shown in Fig. 7b, where $Conv2_1$ of nanogrid 1 is working in MPPT (P&O) mode and generating power around 500W in the start of simulation. At $t=0.027s$, V_B reaches to its maximum allowable limit, therefore, $Conv2_i$ shifts is control from MPPT to current control mode, therefore, the output current of $conv2_i$ i.e. I_1^{in} coincides with load current I_1^{PV} waveform as shown in Fig. 7b. This has been also shown in Fig. 7c where, SOC_i of each converter is increasing due to PV generation higher than load requirements, when V_B is below V_H. After V_B becomes equal to V_H, due to change in control mode of $Conv2_1$ and associated limited PV generation, the SOC of the battery does not rise any further and becomes constant onwards.

6) All nanogrids are below threshold of SOC and PV generation is not available

In order to validate the scenario *g* of section IV, In this case the batteries of all nanogrids are assumed to be below threshold level and PV generation is not available, i.e. $SOC_i < SOC_{min}$; $\forall i=1, 2, 3, 4$. Since PV generation is not available and all the batteries are already blow minimum threshold SOC_{min}, therefore, any local load demand can further discharge batteries and cause DC bus voltage to collapse below minimum threshold level V_L. Therefore, all the local loads are turned off in this condition through a relay and DC bus voltage is limited to lower threshold of voltage V_L through I-V droop with constant droop coefficient given by (5) and also shown in Fig. 2c (Mode 2). Thus, any further power sharing among the contributing nanogrids is restricted to maintain the bus voltage level and battery SOC_i level of individual batteries as shown in Fig 8. This condition is maintained until PV irradiance and associated PV generation is available again to charge the batteries above SOC_{min}.
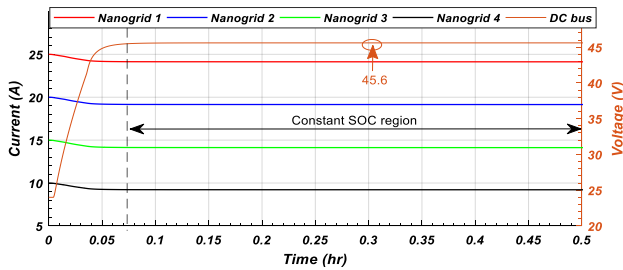

Fig. 8. DC bus voltage V_B profile (righy Y-axis) and battery SOC for contributing nanogrids (SOC_1, SOC_2, SOC_3 and SOC_4) (left Y-axis) in case 6 (simulation results)

B. Experimental Results for the Validation of Proposed Adaptive Algorithm for Conv1i

In order to validate the proposed decentralized control scheme, hardware in loop (HIL) experimentation is conducted using Danfoss converters and dSpace RTI 1006 platform capable to perform real time data acquisition and control operations [29]. The functioning of adaptive algorithm for the control of $Conv1_i$ (shown in Fig. 2c) is evaluated, whose schematics and hardware setup is shown in Figs. 9a and 9b respectively. PV power is emulated using power supply and battery model is emulated using (1) and (2). Since functioning of $Conv2_i$ is to ensure optimal PV generation, while, in the current setup PV power is being emulated, therefore, control of $Conv2_i$ is not implemented for experimentation. Various parameters of experimentations are further detailed in Table II.
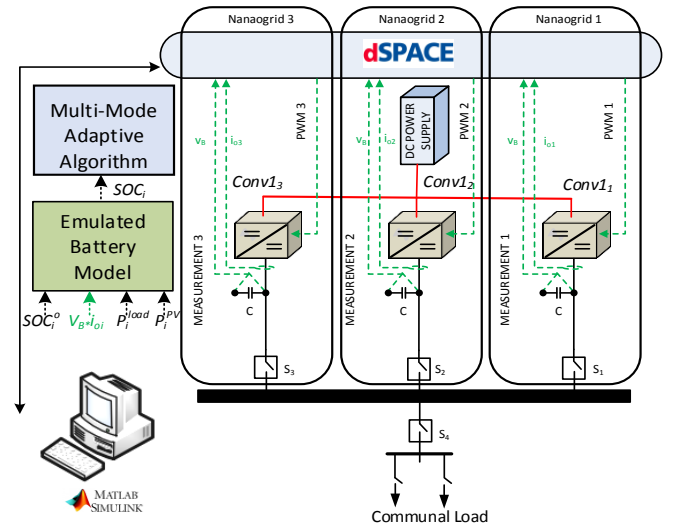

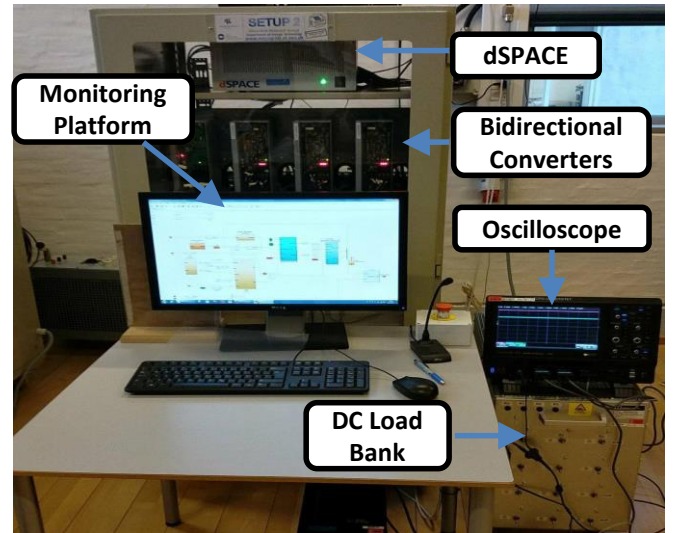Fig. 9a. Schematics of experimental setup at microgrid laboratory

Fig. 9b. Hardware setup for practical measurements

TABLE II
PARAMETERS OF EXPERIMENTAL CASE STUDY

Description of the Parameter	Symbol	Value	Description of the Parameter	Symbol	Value
No. of Nanogrids/ households	N	3	Maximum threshold of battery SOC	SOC_{max}	80%
DC bus capacitance	C_B	3.3mF	Minimum threshold of battery SOC	SOC_{min}	30%
Inductance of each $Conv1_i$	L_I	8.6H	Reference voltage for DC bus	V_{ref}	48V
Stray resistance for Inductors	r_i	0.1Ω	Initial Voltage of DC bus	V_{B0}	24V
Switching frequency for $Conv1i$	f_{sw}	10kHz	Lower limit on DC bus voltage	V_L	45.6V
Rated power of each PV panel	P^{PV}	500W$_p$	Higher limit on DC bus voltage	V_H	50.4V
Rated household load	P^{load}	200W	Proportional and integral parameters ($Conv1_i$)	k_p, k_i	0.02, 0.1
Battery capacity for each nanogrid	C	2400Wh	Droop Coefficient for $Conv1_i$	R_d	0.25Ω
Rated charging current for battery	I_{rated}	5A			

1) All nanogrids are within specified thresholds of SOC

In this scenario, the batteries of all nanogrids are assumed to be within specified thresholds of SOC i.e. $SOC_{min} \leq SOC_i \leq SOC_{max}$; $\forall i=1,2, 3$. This case is evaluated with and without communal load of 135W and results for variations in bus voltage, current sharing among contributing nanogrids and accelerated simulations (1 hr) for SOC_i are shown in Figs. 10a and 10b respectively. Measured results are in accordance with the simulation results as without communal load, the current sharing among the contributing nanogrids is almost zero (slightly higher than zero due to ESR of individual capacitors, which otherwise was zero in case of simulation result due to ideal capacitor). Upon application of communal load, the current sharing is in proportional to SOC_i value. For instance, battery of nanogrid 1 with initial $SOC_1^0=35\%$ is supplying 0.79 A, nanogrid 2 with initial $SOC_2^0=55\%$ is supplying 1.05 A, and nanogrid 3 with initial $SOC_3^0=75\%$ is supplying 1.33 A for communal load application.
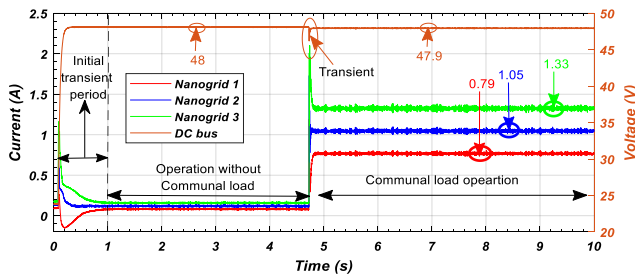
The change in SOC is also in accordance with the SOC availability i.e. $\Delta SOC_1 = 0.49$ %, $\Delta SOC_2 = 0.66$ % and $\Delta SOC_3 = 0.84$ %. Also the initial transition and transition from no load to communal load scenario is fast and smooth as shown in Figs. 10a and 10b respectively.

2) All nanogrids are within specified thresholds of SOC except one which is above maximum threshold of SOC

In this scenario, the batteries of three nanogrids are assumed to be within specified thresholds of SOC, while battery of fourth nanogrid is above maximum threshold, i.e. $SOC_{min} \leq SOC_j \leq SOC_{max}$; $\forall i= 2, 3; SOC_1 > SOC_{max}$. Results for bus voltage profile, current sharing among contributing nanogrids and accelerated simulations (1 hour) for SOC_i are shown in Figs. 11a and 11b respectively. Results verify that the nanogrid 1 having SOC higher than maximum threshold is the supplying nanogrid while remaining two nanogrids demand according to their resource availability.
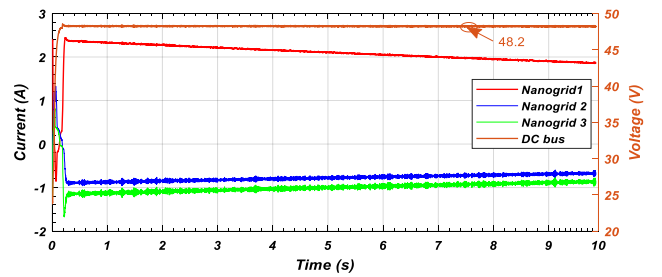
Fig. 10a. DC bus voltage V_B profile (righy Y-axis) and current sharing among nanogrids (I_1^L, I_2^L and I_3^L) (left Y-axis) in case 1 (measured results)
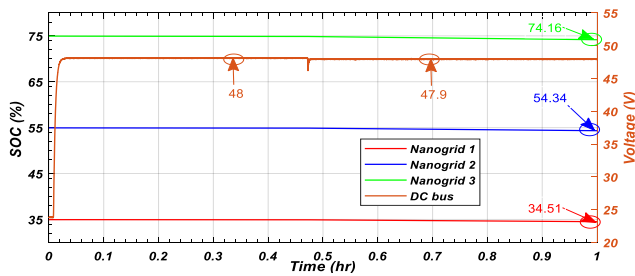

Fig. 11a. DC bus voltage V_B profile (righy Y-axis) and current sharing among nanogrids (I_1^L, I_2^L and I_3^L) (left Y-axis) in case 2 (measured results)

Fig. 10b. DC bus voltage V_B profile (righy Y-axis) and battery SOC for contributing nanogrids (SOC_1, SOC_2, SOC_3 and SOC_4) (left Y-axis) in case 1 (measured results)

Fig. 11b. DC bus voltage V_B profile (righy Y-axis) and battery SOC for contributing nanogrids (SOC_1, SOC_2, SOC_3 and SOC_4) (left Y-axis) in case 2 (measured results)

Nanogrid 2 with higher value of initial SOC_2^0=60% is absorbing relatively lower current in comparison to nanogrid 3 having higher value of initial SOC_2^0=40%. Therefore, change in SOC for absorbing nanogrids from start till end of the simulation is in accordance with resource availability i.e. $\Delta SOC_2 = 0.95\%$ and $\Delta SOC_3 = 1.2\%$ with $(\Delta SOC_3 > \Delta SOC_2)$.
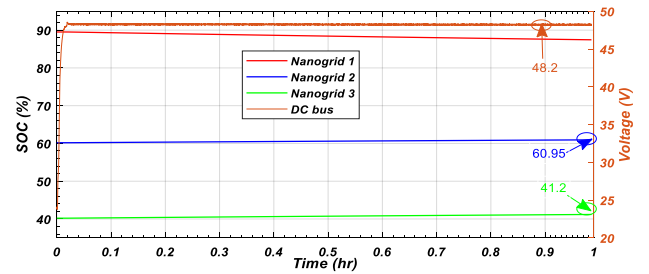
3) Multi-mode switching of an individual Nanogrid

Nanogrids 2 and 3 are considered to be working within specified maximum and minimum thresholds of SOC with $SOC_2<SOC_3$ while, nanogrid 1 is considered below threshold in the start of simulation. It is assumed that PV power produced within nanogrids 2 and 3 is in accordance with their household load, while PV power produced within nanogrid 1 is higher than its household load requirements. Therefore, based upon the emulated model of battery, SOC_1 will increase from values below SOC_{min} to values above $SOC_{max,}$ and $Conv1_1$ will switch its operating modes accordingly.

Fig. 12 shows the variations in current sharing among contributing nanogrids (I_1^L, I_2^L, and I_3^L) based upon the accelerated SOC variations of an individual nanogrid (SOC_1). Accelerated SOC variations at nanogrid 1 are achieved by considering reduced battery capacity (C/10). From Fig. 12, it can be observed that for region $SOC_1 < SOC_{min}$, nanogrid 1 is demanding current with negative value of I_1^L and nanogrid 2 and 3 are supplying in proportion to their SOC, therefore, battery of nanogrid 3 having initial $SOC_3^{(0)}$=60% is supplying more current in this region in comparison to nanogrid 2 having $SOC_2^{(0)}$ =40%. This is in accordance with the simulation results shown in Fig. 6 and I-V droop function as shown in Fig. 2c (Mode 5). The slope of droop increases with SOC in this particular region as shown by the arrow in Fig. 12, which is in accordance with equation discharging droop coefficient $K_d(SOC_i, R_d)$ given by (11). For intermediate region, the current contribution from each nanogrid becomes zero; therefore, it also validates our consideration of almost zero distribution losses in the range of $SOC_{min} \leq SOC_i \leq SOC_{max}$. Finally, in the region when $SOC_i > SOC_{max}$, nanogrid 1 start supplying current with positive value of I_1^L, while nanogrid 2 and nanogrid 3 absorb power in proportion to their resource deficiency. Current sharing is controlled by charging droop coefficient $K_c(SOC_i, R_d)$ given by (9) and shown in Fig. 2c (Mode 5), such that nanogrid 3 having $SOC_3^{(0)} = 60\%$ is absorbing less current in this region in comparison to nanogrid 2 having $SOC_2^{(0)}$ =40%.
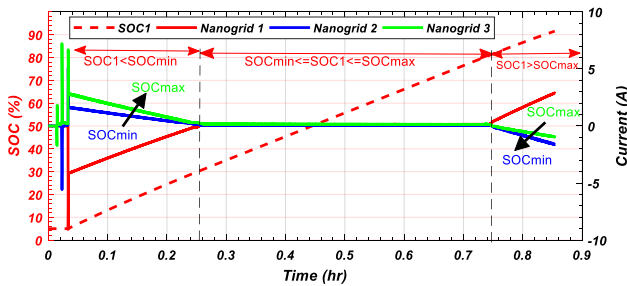

Fig. 12. Nanogrid 1 SOC_1 variations in the various threshold ranges (left Y-axis) and associated current sharing among the contributing nanogrids (right Y- axis) in case 3 (measured results).

VI. CONCLUSION

An adaptive I-V droop method for the decentralized control of a PV/Battery-based distributed architecture of an islanded DC microgrid is presented and its validity is demonstrated with simulations and hardware in loop experimentation. The stability of islanded microgrid in critical operation conditions is ensured via controlled synchronization between generation resources and load requirements. The proposed control method is highly suitable for the rural electrification of developing regions because it (i) enables coordinated distribution of generation and storage resources at a village scale, (ii) reduces distribution losses associated with delivery of energy between generation and load end; (iii) decentralized controllability omits the need of central controller and associated costly communication infrastructure, and (iv) enables resource sharing among the community to extract the benefit of usage diversity at a village scale. Results have also shown that adaptive I-V droop algorithm enables fast and smooth transitions among various modes of microgrid operation based upon the resource availability in individual households of the village. Therefore, the implementation of proposed control method on PV/battery based DGDSA of islanded DC microgrid will enable high efficiency and better resource utilization in future rural electrification implementations.

REFERENCES

[1] World Energy Outlook (WEO, 2016), Electricity Access Database [Online]. Available: http://www.worldenergyoutlook.org/resources/energydevelopment/energyaccessdatabase/.

[2] K. Ubilla *et al.*, "Smart microgrids as a solution for rural electrification: Ensuring long-term sustainability through cadastre and business models," *IEEE Transactions on Sustainable Energy,* vol. 5, no. 4, pp. 1310-1318, 2014.

[3] N. J. Williams, P. Jaramillo, J. Taneja, and T. S. Ustun, "Enabling private sector investment in microgrid-based rural electrification in developing countries: A review," *Renewable and Sustainable Energy Reviews,* vol. 52, pp. 1268-1281, 2015.

[4] S. C. Bhattacharyya, "Financing energy access and off-grid electrification: A review of status, options and challenges," *Renewable and Sustainable Energy Reviews,* vol. 20, pp. 462-472, 2013.

[5] J. J. Justo, F. Mwasilu, J. Lee, and J.-W. Jung, "AC-microgrids versus DC-microgrids with distributed energy resources: A review," *Renewable and Sustainable Energy Reviews,* vol. 24, pp. 387-405, 2013.

[6] J. Khan and M. H. Arsalan, "Solar power technologies for sustainable electricity generation–A review," *Renewable and Sustainable Energy Reviews,* vol. 55, pp. 414-425, 2016.

[7] K. Shenai, A. Jhunjhunwala, and P. Kaur, "Electrifying India: Using solar dc microgrids," *IEEE Power Electronics Magazine,* vol. 3, no. 4, pp. 42-48, 2016.

[8] P. A. Madduri, J. Poon, J. Rosa, M. Podolsky, E. A. Brewer, and S. R. Sanders, "Scalable DC Microgrids for Rural Electrification in Emerging Regions," *IEEE Journal of Emerging and Selected Topics in Power Electronics,* vol. 4, no. 4, pp. 1195-1205, 2016.

[9] S. Mishra and O. Ray, "Advances in nanogrid technology and its integration into rural electrification in India," in *Power Electronics Conference (IPEC-Hiroshima 2014-ECCE-ASIA), 2014 International*, 2014, pp. 2707-2713: IEEE.

[10] D. Palit, G. K. Sarangi, and P. Krithika, "Energising Rural India Using Distributed Generation: The Case of Solar Mini-Grids in Chhattisgarh State, India," in *Mini-Grids for Rural Electrification of Developing Countries*: Springer, 2014, pp. 313-342.

[11] D. Palit and G. K. Sarangi, "Renewable energy based mini-grids for enhancing electricity access: Experiences and lessons from India," in

International Conference and Utility Exhibition on Green Energy for Sustainable Development (ICUE),\ 19-21 March 2014, pp. 1-8.

[12] J. Urpelainen, "Energy poverty and perceptions of solar power in marginalized communities: Survey evidence from Uttar Pradesh, India," *Renewable Energy,* vol. 85, pp. 534-539, 2016.

[13] M. Nasir, N. A. Zaffar, and H. A. Khan, "Analysis on central and distributed architectures of solar powered DC microgrids," in *2016 Clemson University Power Systems Conference (PSC)*, 2016, pp. 1-6.

[14] S. Groh, D. Philipp, B. E. Lasch, and H. Kirchhoff, "Swarm electrification-Suggesting a paradigm change through building microgrids bottom-up," in *Developments in Renewable Energy Technology (ICDRET), 2014 3rd International Conference on the*, 2014, pp. 1-2: IEEE.

[15] W. Inam, D. Strawser, K. K. Afridi, R. J. Ram, and D. J. Perreault, "Architecture and system analysis of microgrids with peer-to-peer electricity sharing to create a marketplace which enables energy access," in *Power Electronics and ECCE Asia (ICPE-ECCE Asia), 2015 9th International Conference on*, 2015, pp. 464-469: IEEE.

[16] P. A. Madduri, J. Rosa, S. R. Sanders, E. A. Brewer, and M. Podolsky, "Design and verification of smart and scalable DC microgrids for emerging regions," in *Energy Conversion Congress and Exposition (ECCE), 2013 IEEE*, 2013, pp. 73-79: IEEE.

[17] P. A. Madduri, J. Poon, J. Rosa, M. Podolsky, E. Brewer, and S. R. Sanders, "Scalable DC Microgrids for Rural Electrification in Emerging Regions," *IEEE Journal of Emerging and Selected Topics in Power Electronics,* vol. PP, no. 99, pp. 1-1, 2016.

[18] J. Chi, W. Peng, X. Jianfang, T. Yi, and C. Fook Hoong, "Implementation of Hierarchical Control in DC Microgrids," *Industrial Electronics, IEEE Transactions on,* vol. 61, no. 8, pp. 4032-4042, 2014.

[19] T. Dragičević, J. M. Guerrero, J. C. Vasquez, and D. Škrlec, "Supervisory control of an adaptive-droop regulated DC microgrid with battery management capability," *IEEE Transactions on Power Electronics,* vol. 29, no. 2, pp. 695-706, 2014.

[20] Q. Shafiee, T. Dragičević, J. C. Vasquez, and J. M. Guerrero, "Hierarchical control for multiple DC-microgrids clusters," *IEEE Transactions on Energy Conversion,* vol. 29, no. 4, pp. 922-933, 2014.

[21] J. M. Guerrero, J. C. Vasquez, J. Matas, L. G. De Vicuña, and M. Castilla, "Hierarchical control of droop-controlled AC and DC microgrids—A general approach toward standardization," *IEEE Transactions on Industrial Electronics,* vol. 58, no. 1, pp. 158-172, 2011.

[22] M. Nasir, H. A. Khan, A. Hussain, L. Mateen, and N. A. Zaffar, "Solar PV-Based Scalable DC Microgrid for Rural Electrification in Developing Regions," *IEEE Transactions on Sustainable Energy,* vol. 9, no. 1, pp. 390-399, 2018.

[23] X. Lu, K. Sun, J. M. Guerrero, J. C. Vasquez, and L. Huang, "State-of-charge balance using adaptive droop control for distributed energy storage systems in DC microgrid applications," *IEEE Transactions on Industrial Electronics,* vol. 61, no. 6, pp. 2804-2815, 2014.

[24] Z. Jin, L. Meng, and J. M. Guerrero, "Comparative admittance-based analysis for different droop control approaches in DC microgrids," in *DC Microgrids (ICDCM), 2017 IEEE Second International Conference on*, 2017, pp. 515-522: IEEE.

[25] F. Gao *et al.*, "Comparative stability analysis of droop control approaches in voltage-source-converter-based DC microgrids," *IEEE Transactions on Power Electronics,* vol. 32, no. 3, pp. 2395-2415, 2017.

[26] B. Subudhi and R. Pradhan, "A comparative study on maximum power point tracking techniques for photovoltaic power systems," *Sustainable Energy, IEEE transactions on,* vol. 4, no. 1, pp. 89-98, 2013.

[27] M. Nasir and M. F. Zia, "Global maximum power point tracking algorithm for photovoltaic systems under partial shading conditions," in *Power Electronics and Motion Control Conference and Exposition (PEMC), 2014 16th International*, 2014, pp. 667-672.

[28] M. Nasir, S. Iqbal, and H. A. Khan, "Optimal Planning and Design of Low-Voltage Low-Power Solar DC Microgrids," *IEEE Transactions on Power Systems,* 2017.

[29] L. Meng, M. Savaghebi, F. Andrade, J. C. Vasquez, J. M. Guerrero, and M. Graells, "Microgrid central controller development and hierarchical control implementation in the intelligent microgrid lab of Aalborg University," in *Applied Power Electronics Conference and Exposition (APEC), 2015 IEEE*, 2015, pp. 2585-2592: IEEE.

Mashood Nasir received his BS degree in Electrical Engineering from UET Lahore, Pakistan and MS in Electrical Engineering from UMT Lahore, Pakistan in 2009 and 2011 respectively. From 2011 to 2012, he served as a lecturer and from 2013-2014 he served as an assistant professor in Electrical Engineering department at UMT, Lahore. From, May 2017 to Nov 2017 he was a visiting PhD researcher at the Microgrid Laboratory in Aalborg University Denmark. Currently, he is a PhD candidate in department of electrical Engineering at LUMS. His research interests mainly include but not limited to power electronics, electrical machines and drives, grid integration of alternate energy resources, electrochemical energy conversion and battery storage systems and AC/DC/Hybrid microgrids.

Zheming Jin (S'15) received the B.S. degree in electrical engineering and the M.S. degree in power electronics and ac drives from Beijing Jiaotong University, Beijing, China, in 2013 and 2015, respectively. He is currently working toward the Ph.D. degree in power electronic systems with the Department of Energy Technology, Aalborg University, Aalborg, Denmark. His research interests include control of power electronic converters, stability of power electronic systems, energy storage, dc microgrids, and their applications in transportation electrification.

Dr. Khan received the B.Eng degree in electronic engineering from GIKI, Pakistan in 2005. From 2005 to 2010, he was with School of Electrical Engineering, The University of Manchester, UK where he first received his MSc (with distinction) and then PhD in electrical and electronic engineering. He is currently serving as assistant professor in the department of Electrical Engineering at LUMS. His current research is on renewable energy and its uptake in developing countries. His core focus is on novel grid architectures for low-cost rural electrification through solar energy. He is also working on efficient and reliable solar PV deployments in urban settings to maximize their performance ratios.

Prof. Nauman Ahmad Zaffar currently serves as Associate Professor and Director of Energy and Power Systems Research Cluster at Department of Electrical Engineering, SBASSE, LUMS, Lahore, Pakistan. His areas of research include smart grids and power electronic converters for integration of renewable energy resources and motor loads with an increasingly smarter grid. His primary research focus is on harnessing and efficient utilization of energy from available sources such as solar PV, solar thermal, wind and hydrokinetics to enable energy independent, integrated, smart grid communities. He has been actively engaged in arranging and delivering national workshops in core areas of circuits, electronics, power electronics and design of magnetics

Juan C. Vasquez (M'12-SM'14) received the B.S. degree in electronics engineering from the Autonomous University of Manizales, Manizales, Colombia, and the Ph.D. degree in automatic control, robotics, and computer vision from the Technical University of Catalonia, Barcelona, Spain, in 2004 and 2009, respectively. He was with the Autonomous University of Manizales working as a teaching assistant and the Technical University of Catalonia as a Post-Doctoral Assistant in 2005 and 2008 respectively. In 2011, he was Assistant Professor and from 2014 he is working as an Associate Professor at the Department of Energy Technology, Aalborg University, Denmark where he is the Vice Program

Leader of the Microgrids Research Program (see microgrids.et.aau.dk). From Feb. 2015 to April 2015 he was a Visiting Scholar at the Center of Power Electronics Systems (CPES) at Virginia Tech and a visiting professor at Ritsumeikan University, Japan. His current research interests include operation, advanced hierarchical and cooperative control, optimization and energy management applied to distributed generation in AC/DC Microgrids, maritime microgrids, advanced metering infrastructures and the integration of Internet of Things and Cyber-Physical Systems into the Smart Grid. He has authored and co-authored more than 100 technical papers only in Microgrids in international IEEE conferences and journals.

Josep M. Guerrero (S'01–M'04–SM'08–FM'15) received the B.S. degree in telecommunications engineering, the M.S. degree in electronics engineering, and the Ph.D. degree in power electronics from the Technical University of Catalonia, Barcelona, Spain, in 1997, 2000, and 2003, respectively. Since 2011, he has been a Full Professor in the Department of Energy Technology, Aalborg University, Aalborg, Denmark, where he is responsible for the Microgrid Research Program. Since 2012, he has been a Guest Professor at the Chinese Academy of Science, Beijing, China and the Nanjing University of Aeronautics and Astronautics, Nanjing, China; since 2014, he has been the Chair Professor in Shandong University, Jinan, China; since 2015, he has been a Distinguished Guest Professor in Hunan University, Changsha, China; and since 2016, he has been a visiting Professor Fellow in Aston University, Birmingham, U.K. His research interest is oriented to different microgrid aspects, including power electronics, distributed energy-storage systems, hierarchical and cooperative control, energy management systems, smart metering and the Internet of things for ac/dc microgrid clusters and islanded minigrids; current research interest especially focused on maritime microgrids for electrical ships, vessels, ferries, and seaports. Prof. Guerrero is an Associate Editor of the IEEE TRANSACTIONS ON POWER ELECTRONICS, the IEEE TRANSACTIONS ON INDUSTRIAL ELECTRONICS, and the IEEE INDUSTRIAL ELECTRONICS MAGAZINE, and an Editor of the IEEE TRANSACTIONS ON SMART GRID and the IEEE TRANSACTIONS ON ENERGY CONVERSION. He was the Chair of the Renewable Energy Systems Technical Committee of the IEEE Industrial Electronics Society. He received the IEEE TRANSACTIONS ON ENERGY CONVERSION Best Paper Award for the period 2014–2015. In 2014 and 2015, he received the Highly Cited Researcher Award by Thomson Reuters, and in 2015, he was elevated as the IEEE Fellow.